



OPEN

Emission Enhancement of Sound Emitters using an Acoustic Metamaterial Cavity

Kyungjun Song¹, Seong-Hyun Lee², Kiwon Kim³, Shin Hur¹ & Jedo Kim⁴

SUBJECT AREAS:

APPLIED PHYSICS

MECHANICAL ENGINEERING

Received
18 November 2013Accepted
31 January 2014Published
3 March 2014Correspondence and
requests for materials
should be addressed to
K.S. (songk@kimm.re.
kr) or J.K. (jedokim@
pknu.ac.kr)

¹Department of Nature-Inspired Nanoconvergence Systems, Korea Institute of Machinery and Materials, 156 Gajeongbuk-Ro, Daejeon, 305-343, Korea, ²Department of System Dynamics, Korea Institute of Machinery and Materials, 156 Gajeongbuk-Ro, Daejeon, 305-343, Korea, ³Department of Mechanical Engineering, Korea Advanced Institute of Science and Technology, 291 Daehak-Ro, Yuseong-Gu, Daejeon, 305-701, Korea, ⁴Department of Mechanical Engineering, Pukyong National University, 365 Sinsun-Ro, Nam-Gu, Busan, 608-739, Korea.

The emission enhancement of sound without electronic components has wide applications in a variety of remote systems, especially when highly miniaturized (smaller than wavelength) structures can be used. The recent advent of acoustic metamaterials has made it possible to realize this. In this study, we propose, design, and demonstrate a new class of acoustic cavity using a double-walled metamaterial structure operating at an extremely low frequency. Periodic zigzag elements which exhibit Fabry-Perot resonant behavior below the phononic band-gap are used to yield strong sound localization within the subwavelength gap, thus providing highly effective emission enhancement. We show, both theoretically and experimentally, 10 dB sound emission enhancement near 1060 Hz that corresponds to a wavelength approximately 30 times that of the periodicity. We also provide a general guideline for the independent tuning of the quality factor and effective volume of acoustic metamaterials. This approach shows the flexibility of our design in the efficient control of the enhancement rate.

Sound emission enhancement dates back to the late 19th and early 20th centuries before any electronic components were invented. During this pre-electronic era, emission enhancement of sound emitters was accomplished purely via mechanical means by utilizing a diaphragm, an air-gate, and compressed air. This form of sound emission enhancement quickly disappeared when a highly effective electronic form was introduced. Nevertheless, emission enhancement without the help of electronics has promising applications in areas such as remote acoustic sensors, energy harvesting, and acoustic filters in which no internal source of power is available. Limitations arise when the wavelengths become large (i.e., low frequency applications) because to confine and control the acoustic waves, structures with dimensions on the order of the wavelength are required, which may be tens of cm to tens of meters. Fortunately, this obstacle is becoming a thing of the past owing to the introduction of metamaterials^{1–4}.

The success of metamaterials in the Electromagnetic (EM) regime is carrying over to the acoustic regime where applications are being found that range from subwavelength focusing to acoustic cloaking^{5,6}. This is possible because basic acoustic parameters such as the bulk modulus (B) and mass density (ρ) can be tailored by sub-wavelength elements analogous to permittivity and permeability in the EM regime^{7–9}. Fabry-Perot-type (FP) resonance modes operating at low frequency are particularly interesting because they allow for full acoustic transmission similar to the extraordinary optical transmission through a subwavelength periodic aperture^{10–14}. Recently, high-resolution sound imaging up to $1/50^{\text{th}}$ of the wavelength was demonstrated by using near-field propagation inside perforated metallic plates using FP resonance modes¹². In addition to utilizing the resonance modes, acoustic metamaterials can also be used to realize high refractive index of sonic systems by using metal plates with a periodic array of subwavelength cylinders^{15,16}, slits¹⁷, and holes¹⁸. Here, we use these unique properties (FP resonance modes and the enhanced refractive index) of acoustic metamaterials to control the quality factor (Q) and the effective volume (V_{eff}) to demonstrate a new class of acoustic resonator for acoustic emitter enhancement at the subwavelength scale.

Results

Double-walled metamaterial cavity design. We designed a structure composed of two perforated metamaterials with a unit cell size of $a = 10$ mm separated by an air gap of distance $g = 20$ mm to form a so-called double-fishnet structure (Fig. 1a). The elements inside the unit cell have the dimensions of $h = 11$ mm, $s = 3$ mm, $t = 1$ mm, $w = 5$ mm, and a path periodicity of $p = 2.5$, which is defined by the number of oscillatory paths taken by

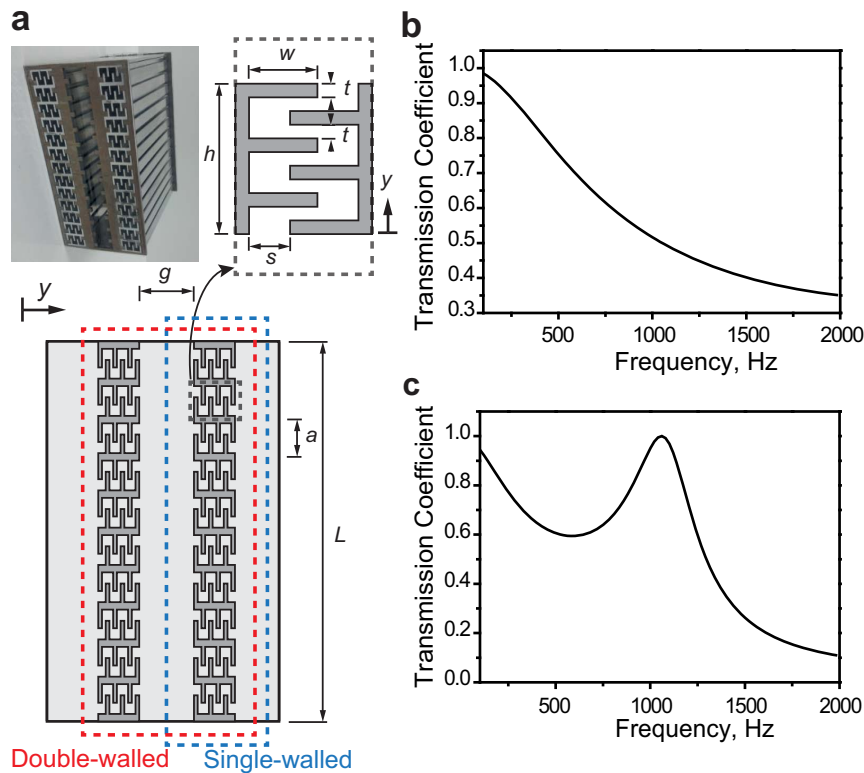


Figure 1 | Design of the metamaterials and predicted transmission coefficients. (a) The double-walled acoustic cavity consisting of a pair of square aluminum metamaterial slabs with perforated elements. The schematic of the unit cell is shown at the top right corner with the dimensions of $w = 0.5$ mm, $t = 1$ mm, $h = 11$ mm, $s = 3$ mm, $g = 20$ mm, $a = 10$ mm, and $L = 100$ mm. $y = 0$ is defined as the location where the incident acoustic wave first encounters the metamaterial. Two independent metamaterial slabs comprise the double-walled cavity with an air gap of g . Transmission coefficient were calculated for the (a) single and (b) double metamaterial slabs using the power intensity results from COMSOL.

the wave along the direction of propagation. Such a design is used to realize the following two distinct characteristics: 1) the unique FP resonance modes that allow for full acoustic transmission with high selectivity and 2) an increased effective refractive index by the increased path of the incoming waves. Independently, these two characteristics are not intriguing, but when these effects are combined, interesting events occur. The increased refractive index shifts the FP resonance modes to low frequencies, where the wavelength becomes much larger than the size of the unit cell. Because no cutoff frequency exists in the acoustic regime, the periodic arrangement yields full acoustic transmission that extends to subwavelength scales. To theoretically predict the frequency response of the metamaterial, we performed numerical calculations using COMSOL, a finite element analysis and solver software package, using incident plane waves in the normal direction. In our calculation, we used a Young's modulus of 8.5×10^9 Pa, a density of 10^{11} kg/m³, and a Poisson's ratio of 0.33 to simulate the mechanical properties of aluminum and chose air as the fluid. The transmission coefficients of the single (Fig. 1b) and the double-walled metamaterial slab (Fig. 1c) indicate that for the single slab, no resonance behavior is expected because the fundamental resonance mode is expected to be approximately 5000 Hz (Fig. S1). However, for the double-walled metamaterial slab, full transmission is expected near 1060 Hz, where the wavelength is significantly larger than the periodicity of the metamaterial structure.

Full transmission of double-walled metamaterials. The 0th mode transmission (t) and the reflection (r) coefficients of the single metamaterial slab can be calculated using the effective medium parameters: effective impedance (Z_{eff}) and effective refractive index (n_{eff}). Under this condition, (the reflected and transmitted pressure is written as $P(x,y) = \exp(jk_x x)[\exp(jk_y y) + r \exp(-jk_y y)]$ for $y > 0$ and

$P(x,y) = t \exp(jk_x x)[\exp(jk_y(y-h))]$ for $y > h$ (Fig. 1a). Inside the oscillatory path, pressure field can be described by the effective medium parameters and is written as $P(x,y) = \exp(jn_{\text{eff}} k_x x) [A \exp(jn_{\text{eff}} k_y y) + B \exp(-jn_{\text{eff}} k_y y)]$ for $0 < y < h$, where A is the amplitude of forward propagating waves and B is the amplitude of backward propagating waves, respectively. By imposing continuity of the pressure field and the normal velocities over the entire slab at $y = 0$ and $y = h$, transmission and reflection coefficients is written as:

$$t = \frac{4Z_1 Z_{\text{eff}}}{[Z_1 + Z_{\text{eff}}][Z_{\text{eff}} + Z_1] e^{-jn_{\text{eff}} kh} + [Z_1 - Z_{\text{eff}}][Z_{\text{eff}} - Z_1] e^{jn_{\text{eff}} kh}}$$

$$r = \frac{[Z_1 + Z_{\text{eff}}][Z_{\text{eff}} + Z_1] e^{-jn_{\text{eff}} kh} + [Z_1 - Z_{\text{eff}}][Z_{\text{eff}} + Z_1] e^{jn_{\text{eff}} kh}}{[Z_1 + Z_{\text{eff}}][Z_{\text{eff}} + Z_1] e^{-jn_{\text{eff}} kh} + [Z_1 - Z_{\text{eff}}][Z_{\text{eff}} - Z_1] e^{jn_{\text{eff}} kh}} \quad (1)$$

where $Z_1 = \frac{\rho c}{\cos \theta}$ (ρ and c are the density and acoustic velocity of air, respectively and θ is the angle of the incident wave with respect to the surface normal). From equation (1), it is apparent that Z_{eff} and n_{eff} determine the transmission and reflection coefficients. Thus, full transmission is expected at the FP resonant condition: $kh = n_{\text{eff}} k_0 h = m\pi$, with m being an integer number. Conversely, sound suppression is to be expected by the odd-mode FP condition: $kh = n_{\text{eff}} k_0 h = (m + 1/2)\pi$, with m being an integer number. We find that the wave number, k , inside the slab is determined by the refractive index $k = k_0 n_{\text{eff}}$, hence it is possible to shift the FP resonance mode to lower frequencies by increasing n_{eff} .

Effective acoustic parameters of double-walled metamaterials. To control n_{eff} , we use periodic zigzag elements as shown in Fig. 1a to yield the effective refractive index n_{eff} . The single slab metamaterial



structure can be regarded as a single film in which n_{eff} and Z_{eff} determines its properties under the condition that the wavelength is much larger than the total thickness of the slab (Fig. 2a). As expected, the effective refractive index of a single slab, as calculated by the acoustic numerical retrieval scattering method^{18,20}, can be tailored by changing the flange width (w) which in turn changes the path length (Fig. 2b). The effective refractive index of our prototype with a flange width $w = 0.5$ mm is found to be approximately $n_{\text{eff}} = 3.0n_0$, where n_0 is the refractive index of air. However, when the flange width is increased to $w = 0.7$ mm, the refractive index becomes as high as $n_{\text{eff}} = 4.0n_0$. These results show that the effective impedance Z_{eff} of the single slab also increases by increasing the path length (Fig. 2c). By using the same logic as used with the single slab, the double-walled slab can be considered a single film determined by its own n_{eff} and Z_{eff} (Fig. 2d). The results show that below 600 Hz ($\lambda = 57.2$ cm), the double slab with $w = 0.5$ mm and $g = 20$ mm exhibits a lower refractive index of $n_{\text{eff}} = 2.7n_0$ compared to that of the single slab (Fig. 2e). However, between frequencies 1000 and 1300 Hz, the refractive index of the double-walled slab exceeds that of the single slab due to the presence of FP resonance. This is analogous to the realization of an extraordinarily high refractive index in the electromagnetic regime by utilizing electron resonances²¹ or the electromagnetic resonances of splitting resonators (SRRs)²⁴. Furthermore, impedance variation of the double-walled slab indicates resonant behavior near 1060 Hz where the real and imaginary impedances become simultaneously close to zero (Fig. 2f). The real part of the effective impedance decreases monotonically up to 1060 Hz, while the imaginary part of effective impedance monotonically increases after 1060 Hz. This behavior can be explained by a simple circuit analogue represented by series inductor-capacitor (LC) coupling process where both a magnitude

and phase exist for the double-walled slab, in contrast to the single slab which has only the magnitude.

Measurement of full transmission with high selectivity. To experimentally verify the full transmission behavior with high selectivity, we perform reflection coefficient measurements upstream of the slab (Figs. 3a–b). These results indicate excellent agreement between the experimental and theoretical values, apart from some discrepancies below 600 Hz. For the single slab, the theory predicts that the fundamental FP resonant mode is expected at approximately 5000 Hz hence, no abrupt change in the reflection coefficient is shown. However, for the double-walled slab, the reflection coefficient decreases to almost zero near 1060 Hz indicating full transmission due to the existence of a FP resonant mode. This resonant mode can be regarded as the fundamental FP resonant condition given by the following equation: $k_0 n_{\text{eff}} \times (2h + g) = \pi$ leading to an $n_{\text{eff}} = 3.8$, because the wavelength $\lambda = 32$ cm (at 1060 Hz). At this frequency, the periodicity is approximately $1/30^{\text{th}}$ of the wavelength, thus providing a highly miniaturized acoustic cavity at the subwavelength scale.

Emission enhancement of sound based on metamaterials. This acoustic cavity with a subwavelength gap can be used to enhance sound similar to luminescence enhancement of an atom in a cavity^{22,23} or proposed phonon density of states enhancement²⁴. The enhancement rate (S) at the resonance mode can be estimated by the quality factor Q and the effective cavity volume V_{eff} ($S \sim Q/V_{\text{eff}}$) analogues to the Purcell effect of EM micro-resonators²⁵. The Q factor determines the sound confinement time in units of acoustic period and V_{eff} measures the effective confinement volume of the resonator²⁶. To theoretically predict and analyze the enhancement rate, we simulated the acoustic enhancement numerically using a 2D

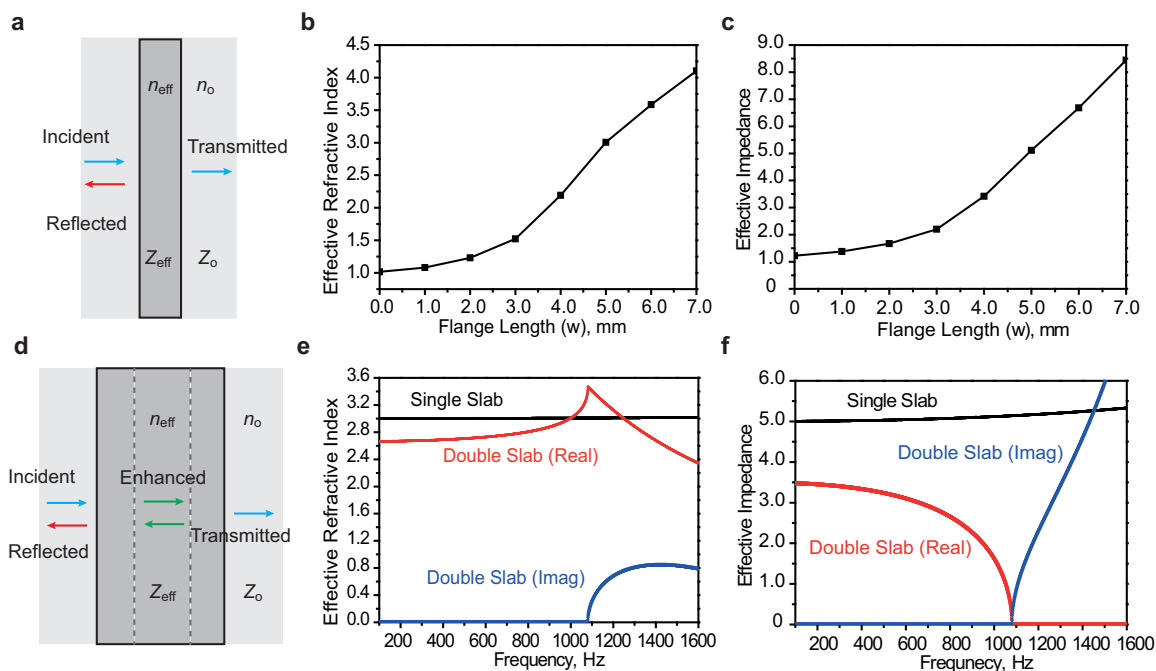


Figure 2 | Effective medium analysis of single and double-walled metamaterial slabs. (a) The perforated metamaterial can be viewed as a single slab using the effective medium theory when the incident wavelength is much larger than the unit cell (0^{th} mode condition). Then effective medium parameters such as effective refractive index n_{eff} and effective impedance Z_{eff} can be used to characterize the transmission and reflection coefficients. Variation of (b) n_{eff} and (c) Z_{eff} with respect to the flange length (w) for the single slab metamaterial calculated using acoustic numerical retrieval scattering method^{18,19} is as shown. Increases in the refractive index and impedance are achieved by an increased path length when w is increased. (d) The double metamaterial slab can also be viewed as a single slab where the effective material parameters arise by coupling between the metamaterial-gap-metamaterial. Calculated (e) effective refractive index and (f) effective impedance of single and double metamaterial slab for frequencies between 100 and 1600 Hz are as shown. The single slab behave as resistive component having only a real component of the effective impedance, while the double slab behave as LC components having both real and imaginary components between 1060 Hz and 1600 Hz.

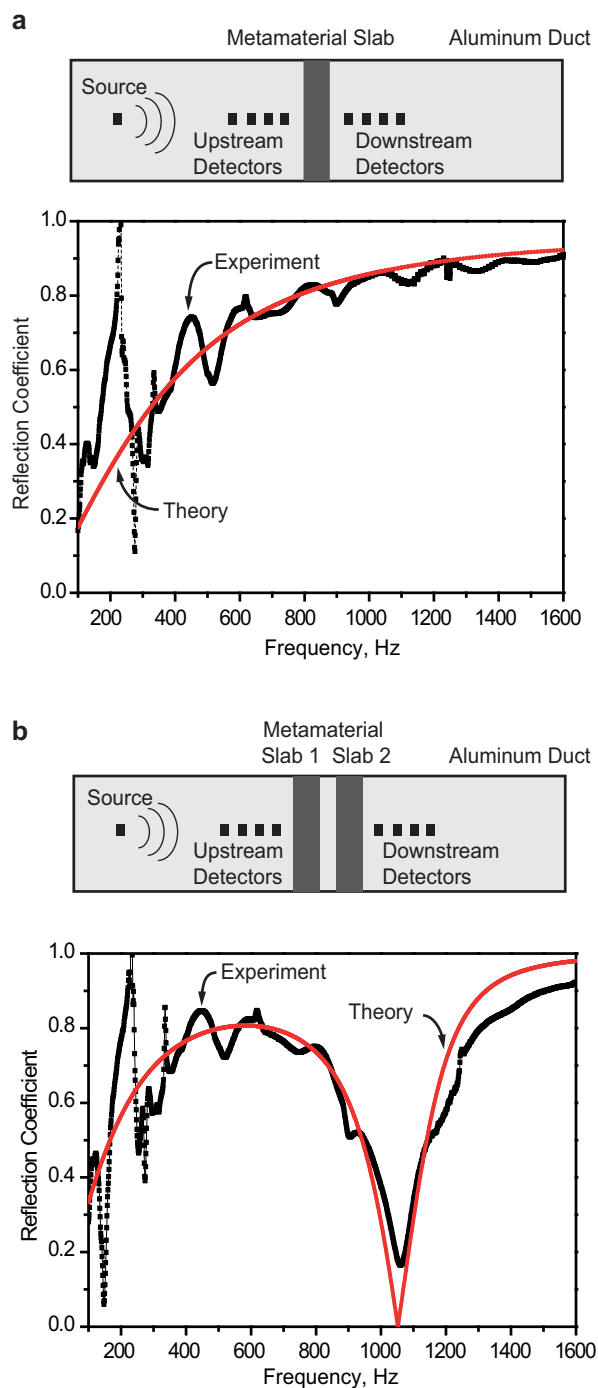


Figure 3 | Reflection coefficient measurement. Measured (black) and calculated (red) reflection coefficients of a (a) single slab and (b) double slab as shown, respectively. The reflection coefficient was measured by an upstream microphone using the source as the reference signal. The transmission loss was measured by a downstream microphone, shown in Fig. S2. The theoretical results were calculated using power intensity values found using the finite element package COMSOL.

double walled cavity with a width of $L = 100$ mm and placed a point source at the center of the cavity. This was compared to the case with no metamaterial cavity. The acoustic intensity field profiles at resonance, at off-resonance, and with no metamaterial clearly show that the acoustic signal at FP resonance is confined within the cavity at the fundamental FP resonance frequency (Figs. 4a–c). The power intensity distribution across the cavity indicates strong local acoustic intensity enhancement inside the low impedance

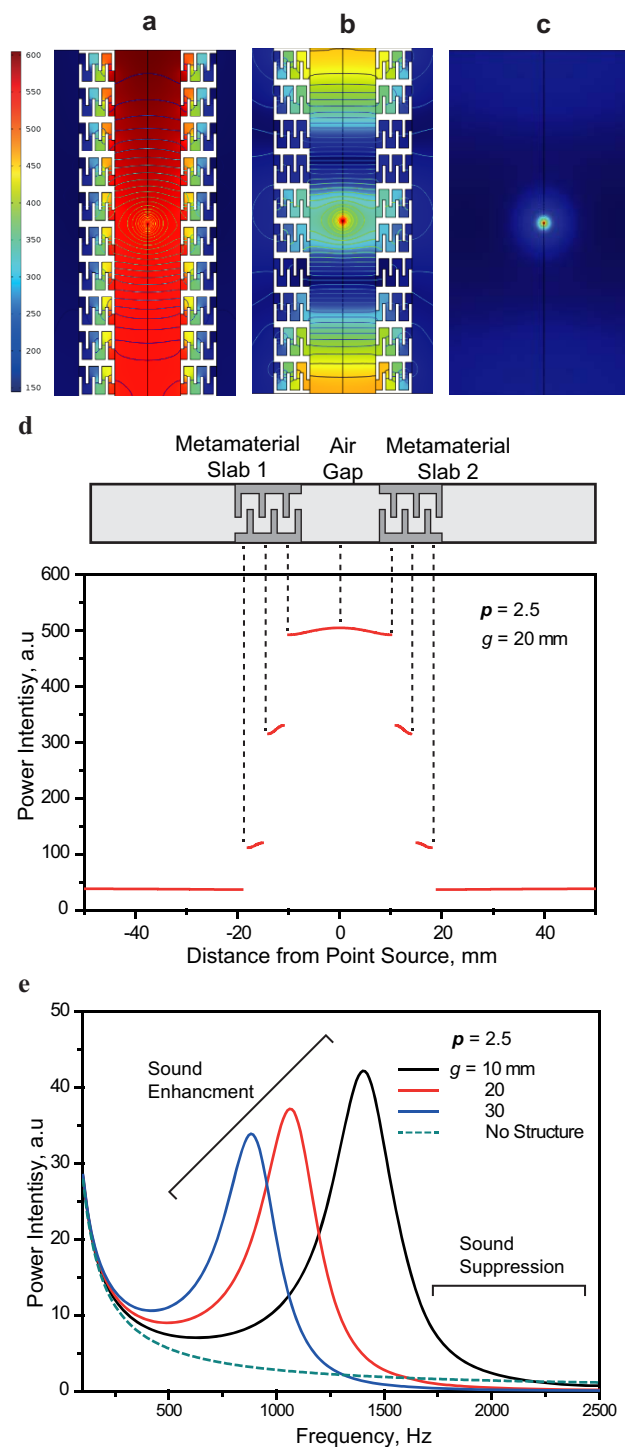


Figure 4 | Theoretical analysis of the double-walled metamaterial cavity. Profiles of the pressure field distribution (a) at acoustic emission enhancement regime (resonant frequency of 1060 Hz), (b) at acoustic suppression regime (above 1060 Hz), and (c) with no structure. A point source was placed inside the cavity so that the intensity was 10 W/m^2 at 0.001 m away from the source. (d) The acoustic pressure intensity distribution within the cavity. The index of impedance discontinuity confines the acoustic field within the low impedance region which results in a significantly low effective volume. (e) Variation of the acoustic intensity with respect to frequency for 3 different air gaps ($g = 10, 20,$ and 30 mm) for $p = 2.5$. Sharp power intensity peaks are shown at the respective fundamental FP resonance modes for different dimensional parameters and sound suppression is predicted above these power intensity peaks.



region reflecting reduced V_{eff} (Fig. 4d). This reduction in the effective volume is caused by impedance discontinuities at the subwavelength scale²⁷ that confine the acoustic field to the low impedance region. The quality factor Q is estimated by using the following relationship: $Q \approx 1/BW$ where BW is the fractional bandwidth and BW of our double-walled slab with $w = 0.5$ mm and $g = 20$ mm, yielding $Q = 2.9$ (see supplementary material). The acoustic power intensity at the location 40 mm from the either side of the outer wall illustrates an approximately 10-fold enhancement at a frequency near 1060 Hz which corresponds to the fundamental FP resonance mode for $p = 2.5$ and $g = 20$ mm (Fig. 4e). When $g = 10$ mm, 20 fold enhancement is achieved near 1500 Hz resulting from the enhancement of the quality factor to $Q = 3.6$ (see supplementary information Table S1) and a reduced effective volume V_{eff} . Q can be further enhanced by increasing the path periodicity p , and the results show that the fundamental FP resonance mode can be shifted to extremely low frequencies (see supplement Fig. S4). As determined by the quality factor calculation results shown in the supplement (Tables S1 and S2), the double-walled cavity with $g = 10$ mm and $p = 5$ show a 2-fold increase in the acoustic power intensity at approximately 900 Hz ($\lambda = 38.2$ cm) due to the simultaneous enhancement and reduction of Q and V_{eff} respectively (Fig. S4). In addition to this enhancement, the results predict sound suppression regime beyond the fundamental FP resonance mode where the sound intensity becomes minimal near 2500 Hz, consistent with the behavior often reported for two adjacent holey plates^{18,28} (Figs. 4e–f and Fig. S3).

Measurement of sound emission enhancement. Next, we performed experiments to directly measure the acoustic field enhancement by using a 3D rectangular cavity structure (cross section 130 mm \times 100 mm and $g = 20$ mm) mounted on a rotating stage with a simulated point source inserted inside the metamaterial cavity (Fig. 5a–b). The sound pressure level (SPL) with P_m and without (P_o) the metamaterial cavity was measured 1.5 m away from the source, and the results show significant sound emission enhancement near 1300 Hz and sound suppression thereafter (Fig. 5c). The maximum SPL gain ($P_m - P_o$) show approximately 10 dB gain; this experimental result (with cavity $g = 20$ mm) is in excellent agreement with the theoretical predictions with a cavity $g = 13$ mm (Fig. 5d). The discrepancy in frequency is attributed to a smaller effective cavity volume caused by the insertion of a cylindrical waveguide which was used to simulate the point source. The smaller effective volume shifts the fundamental FP resonance mode to higher frequencies consistent with the theoretical predictions. We also measure the polar SPL gain by progressively rotating the rectangular cavity by 30 degrees and find that the enhancement is omnidirectional (see Fig. S5 and Fig. S6).

Discussion

We have shown that the designed double-walled metamaterial cavity successfully enhances emission of sound at low frequencies, thus demonstrating a highly miniaturized acoustic cavity. This device uses Fabry-Perot resonance modes for sound enhancement determined by the quality factor Q and effective cavity volume V_{eff} . In addition, optimal design of an acoustic cavity can be obtained by careful design of the number of path periodicity and the gap size. Such versatility makes this structure scalable to be used over a wide range of acoustic frequencies allowing broad applications in many areas where remote systems are used. We hope that such efforts presented here will widen the footprint of metamaterials in the acoustic regime and open doors to many more interesting applications such as acoustic sensors and energy harvesting.

Methods

Prototype fabrication. The periodic zigzag elements were manufactured by computer numerical control (CNC) precision machining. Each slab was inserted within a prefabricated jig made out of aluminum to achieve desired air gap size.

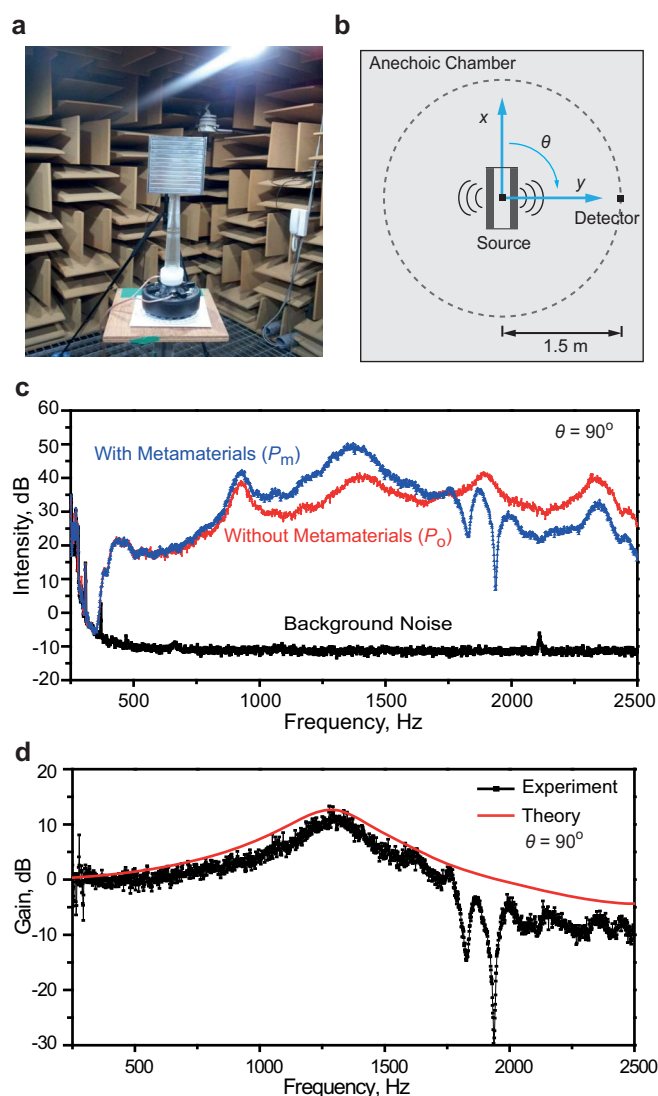


Figure 5 | Sound emission enhancement measurement of the double-walled metamaterial cavity. (a) Photograph and (b) layout of the experimental set-up for measuring the emitted sound pressure outside the metamaterial cavity. To simulate a point source within the cavity, an acrylic cylinder ($d = 15$ mm) was inserted inside the double-walled metamaterial cavity to serve as a waveguide for the sound source located below the prototype. (c) The measured sound intensity with (P_m) and without (P_o) the double-walled metamaterial cavity measured for $\theta = 90^\circ$. Background noise was found to be -10 dB, which yields a high signal-to-noise ratio for the measured values. (d) The acoustic gain calculated by the difference between P_m and P_o for $\theta = 90^\circ$. For the measured values with an air gap $g = 20$ mm, excellent agreement was found with the theoretical values with an air gap $g = 13$ mm. This difference is attributed to the reduced effective volume of the cavity due to the presence of the acrylic cylinder.

Transmission and reflection measurement. A square aluminum duct (inner dimensions of 100 \times 100 mm) was used to enclose the loud speaker (sound source), metamaterial slab (cavity), B&K 4938 quarter inch microphones (detector). The sound source was located 1.0 m upstream of the slab and four detectors were located both upstream and downstream of the slab. The distance between the slab and the closest microphone was 0.1 m and the spacing between the microphones was 0.0415 m. The valid frequency range was from 100 Hz to 1600 Hz, which is limited by both the cut-off frequency of the first acoustic mode and the spacing between the microphones. To eliminate the effects of reflected waves, an anechoic termination was installed at the end of the square duct.

Transmission and reflection analysis. The transmission and reflection calculations were carried out using the COMSOL Multi-physics software package. For a finite-



element model, we assumed the sound wave impinging on the single and double slabs as incidence plane sound waves. Due to the periodicity, we analyzed a unit cell with periodic boundary conditions and used perfectly matched layer (PML) absorbing boundary conditions at the top and bottom boundaries of the unit cell.

Effective mechanical parameters. We used the retrieval scattering method adapted for acoustic metamaterials based on the scattering coefficients calculated by COMSOL Multi-physics software. These coefficients can be calculated by using normally incident sound waves on a single slab and double slabs. We invert the scattering coefficients for calculating n_{eff} and Z_{eff} by using constitutive conditions of passive acoustic medium: $\text{Re}(Z) > 0$ and $\text{Im}(n) > 0$.

Acoustic emission enhancement measurement. The double-walled cavity was placed on a rotating stage at the center of an anechoic chamber. To generate a point-like source inside the metamaterial cavity, sound generated from the compression driver (NSU-50N) was feed through a tiny hole in the resonator by a circular waveguide made of acrylic. The emitted sound pressure was measured by a B&K 4189-A-021 microphone 1.5 m away from the double-walled metamaterial cavity.

- Pendry, J. B., Holden, A. J., Stewart, W. J. & Youngs, I. Extremely low frequency plasmons in metallic mesostructures. *Phys. Rev. Lett.* **76**, 4773–4776 (1996).
- Smith, D. R., Padilla, W. J., Vier, D. C., Nemat-Nasser, S. C. & Schultz, S. Composite medium with simultaneously negative permeability and permittivity. *Phys. Rev. Lett.* **84**, 4184–4187 (2000).
- Pendry, J. B., Holden, A. J., Robbins, D. J. & Stewart, W. J. Magnetism from conductors and enhanced nonlinear phenomena. *IEEE T. Microw. Theory* **47**, 2075–2084 (1999).
- Shelby, R. A., Smith, D. R. & Schultz, S. Experimental verification of a negative index of refraction. *Science* **292**, 77–79 (2001).
- Fang, N. *et al.* Ultrasonic metamaterials with negative modulus. *Nat. Mater.* **5**, 452–456 (2006).
- Zhang, S., Xia, C. & Fang, N. Broadband acoustic cloak for ultrasound waves. *Phys. Rev. Lett.* **106**, 024301 (2011).
- Li, J. & Chan, C. T. Double-negative acoustic metamaterial. *Phys. Rev. E* **70**, 055602 (2004).
- Liu, Z. *et al.* Locally resonant sonic materials. *Science* **289**, 1734–1736 (2000).
- Liang, Z. & Li, J. Extreme acoustic metamaterial by coiling up space. *Phys. Rev. Lett.* **108**, 114301 (2012).
- Lu, M. *et al.* Extraordinary acoustic transmission through a 1D grating with very narrow apertures. *Phys. Rev. Lett.* **90**, 174301 (2007).
- Christensen, J., Fernandez-Dominguez, A. I., De Leon-Perez, F., Martín-Moreno, L. & García-Vidal, F. J. Collimation of sound assisted by acoustic surface waves. *Nat. Phys.* **3**, 851–852 (2007).
- Christensen, J., García-Vidal, F. J., Martín-Moreno, L. & Zhu, J. A holey-structured metamaterial for acoustic deep-subwavelength imaging. *Nat. Phys.* **55**, 52–55 (2011).
- Zhou, Y. *et al.* Acoustic surface evanescent wave and its dominant contribution to extraordinary acoustic transmission and collimation of sound. *Phys. Rev. Lett.* **104**, 164301 (2010).
- Christensen, J., Martín-Moreno, L. & García-Vidal, F. J. Theory of resonant acoustic transmission through subwavelength apertures. *Phys. Rev. Lett.* **101**, 014301 (2008).
- Hu, X. & Chan, C. T. Refraction of water waves by periodic cylinder arrays. *Phys. Rev. Lett.* **95**, 154501 (2005).
- Cervera, F. *et al.* Refractive acoustic devices for airborne sound. *Phys. Rev. Lett.* **88**, 023902 (2001).

- Hu, X., Ho, K.-M., Chan, C. T. & Zi, J. Homogenization of acoustic metamaterials of Helmholtz resonators in fluid. *Phys. Rev. B* **77**, 172301 (2008).
- Christensen, J., Martín-Moreno, L. & García-Vidal, F. J. All-angle blockage of sound by an acoustic double-fishnet metamaterial. *Appl. Phys. Lett.* **97**, 134106 (2010).
- Smith, D. R., Schultz, S., Markoš, P. & Soukoulis, C. M. Determination of effective permittivity and permeability of metamaterials from reflection and transmission coefficients. *Phys. Rev. B* **65**, 195104 (2002).
- Fokin, V., Ambati, M., Sun, C. & Zhang, X. Method for retrieving effective properties of locally resonant acoustic metamaterials. *Phys. Rev. B* **76**, 144302 (2007).
- Scully, M. O. Enhancement of the index of refraction via quantum coherence. *Phys. Rev. Lett.* **67**, 1855–1858 (1991).
- Kleppner, D. Inhibited spontaneous emission. *Phys. Rev. Lett.* **47**, 233–236 (1981).
- Heinzen, D. J., Childs, J. J., Thomas, J. E. & Feld, M. S. Enhanced and inhibited visible spontaneous emission by atoms in a confocal resonator. *Phys. Rev. Lett.* **58**, 1320–1323 (1987).
- Kim, J., Kapoor, A. & Kaviani, M. Material metrics for laser cooling of solids. *Phys. Rev. B* **77**, 115127 (2008).
- J, V. K. Optical microcavities: Photonic technologies. *Nature* **424**, 839–846 (2003).
- Kyungjun, S. & Mazumder, P. Dynamic terahertz spoof surface plasmon polariton switch based on resonance and absorption. *IEEE T. Electron. Dev.* **58**, 2172–2176 (2011).
- Robinson, J. T., Manolatu, C., Chen, L. & Lipson, M. Ultrasmall mode volumes in dielectric optical microcavities. *Phys. Rev. Lett.* **95**, 143901 (2005).
- Bell, J. S. *et al.* Low acoustic transmittance through a holey structure. *Phys. Rev. B* **85**, 214305 (2012).

Acknowledgments

The authors acknowledge the financial support of the Converging Research Center Program through the Ministry of Science, ICT and Future Planning, Korea 2013K000330 and NRF-2013R1A1A1075994.

Author contributions

K.S. and J.K. designed and developed the double-walled acoustic metamaterial for sound enhancement. K.S. and S.H. manufactured the acoustic cavity. S.L. carried out the transmission and reflection measurements. K.K. and K.S. carried out the acoustic enhancement measurements. J.K. and K.S. conducted the numerical simulations and wrote the manuscript.

Additional information

Supplementary information accompanies this paper at <http://www.nature.com/scientificreports>

Competing financial interests: The authors declare no competing financial interests.

How to cite this article: Song, K., Lee, S.-H., Kim, K., Hur, S. & Kim, J. Emission Enhancement of Sound Emitters using an Acoustic Metamaterial Cavity. *Sci. Rep.* **4**, 4165; DOI:10.1038/srep04165 (2014).



This work is licensed under a Creative Commons Attribution-NonCommercial-NoDerivs 3.0 Unported license. To view a copy of this license, visit <http://creativecommons.org/licenses/by-nc-nd/3.0>